Science of the Total Environment 794 (2021) 148692

Contents lists available at ScienceDirect

Science of the Total Environment

journal homepage: www.elsevier.com/locate/scitotenv

Modification of structured bio-carbon derived from spongin-based scaffolds with nickel compounds to produce a functional catalyst for reduction and oxidation reactions: Potential for use in environmental protection

Sonia Żółtowska [a], Zuzanna Bielan [b], Joanna Zembrzuska [c], Katarzyna Siwińska-Ciesielczyk [a], Adam Piasecki [d], Anna Zielińska-Jurek [b], Teofil Jesionowski [a,*]

[a] Poznan University of Technology, Faculty of Chemical Technology, Institute of Chemical Technology and Engineering, Berdychowo 4, PL-60965 Poznan, Poland
[b] Gdansk University of Technology, Faculty of Chemistry, Department of Process Engineering and Chemical Technology, Narutowicza 11/12, PL-80233 Gdansk, Poland
[c] Poznan University of Technology, Faculty of Chemical Technology, Institute of Chemistry and Electrochemistry, Berdychowo 4, PL-60965 Poznan, Poland
[d] Poznan University of Technology, Faculty of Mechanical Engineering and Management, Institute of Materials Science and Engineering, Jana Pawla II 24, PL-60965 Poznan, Poland

HIGHLIGHTS

- Marine sponges as a biomimetic source of biocarbons
- Prepared biocarbons were modified with Ni species to obtain functional materials.
- Study of morphological and physicochemical properties of prepared composites
- Ni-modified biocarbons as functional materials for catalytic use.
- New catalysts for oxidation or reduction reactions of phenolic compounds

GRAPHICAL ABSTRACT

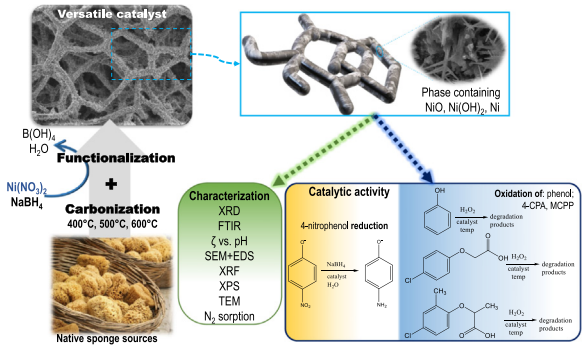

ARTICLE INFO

Article history:
Received 1 March 2021
Received in revised form 27 May 2021
Accepted 22 June 2021
Available online 28 June 2021

Editor: Daniel CW Tsang

Keywords:
Organic-based wastewater treatment
Spongin-based scaffolds
Carbonization
Nickel-based catalysts
Noble-metal-free catalysts
Oxidation and reduction reactions

ABSTRACT

Three different 3D fibrous-like NiO/Ni(OH)$_2$/Ni-carbonized spongin-based materials were prepared via a simple sorption–reduction method. Depending on the support used, the catalysts were composed of carbon, nickel oxide, nickel hydroxide and zero-valent nickel, with the surface content of the nickel-containing phase in the range 15.2–26.0 wt%. Catalytic studies showed promising activity in the oxidation of phenolic compounds in water and in the reduction of 4-nitrophenol. The oxidation efficiency depends on the substrate used and ranges from 80% for phenol at pH 2 to 99% for 4-chlorophenoxyacetic acid (4-CPA) and methylchlorophenoxypropionic acid (MCPP). In the reduction reaction, all catalysts exhibited superior activity, with rate constants in the range 0.648–1.022 min^{-1}. The work also includes a detailed investigation of reusability and kinetic studies.

* Corresponding author.
E-mail address: Teofil.Jesionowski@put.poznan.pl (T. Jesionowski).

https://doi.org/10.1016/j.scitotenv.2021.148692

1. Introduction

In recent decades, much attention has been paid to various methods of water remediation, including sorption (Abdel Maksoud et al., 2020; Ahsan et al., 2020; Bartczak et al., 2018; El-Sayed, 2020; Fang et al., 2020; Żółtowska-Aksamitowska et al., 2018), ozonation (Schmitt et al., 2020), photocatalytic and catalytic approaches (Acharya and Parida, 2020; Fang et al., 2020; Kubiak et al., 2020; Kumari et al., 2020; X. Liu et al., 2020b; Lu and Astruc, 2020; Siwińska-Ciesielczyk et al., 2020), membrane separation and sedimentation (Chen et al., 2020). However, each method has drawbacks and may lead to the production of problematic wastes requiring safe and efficient disposal. Although there is no universal solution to these problems, catalysis currently seems to have a crucial role in the development of effective processes and methods that can maximize effectiveness and minimize waste generation and energy demand (De et al., 2016).

Particular interest is focused on metal-based catalysts, which have been extensively utilized in a wide range of applications (Finiels et al., 2014; Lee and Lee, 2020; H. Liu et al., 2020a; Ma et al., 2019; Yan et al., 2016; Yang et al., 2019; Zhang et al., 2007; Zheng et al., 2017; Zuo et al., 2016), including biotechnological treatment processes (El-Sayed, 2020; Jankowska et al., 2019; Zdarta et al., 2019). Such materials have been investigated in particular with regard to their use in oxidation–reduction reactions of organic compounds (Ambursa et al., 2021; Parmeggiani and Cardona, 2012). For comparison, Table 1 presents a set of studies on the catalytic oxidation of phenol and its derivatives and the reduction of 4-nitrophenol using various metal-based catalysts.

As shown above, heterogeneous catalysis offers endless possibilities in the degradation of organic compounds via either oxidation or reduction reactions. Recent results have proved the usefulness of a wide range of materials in the removal of phenolic compounds from water and wastewater. It is notable that composites based on transition metals are most commonly used in the degradation of organic compounds (Verdine, 2019).

Among the metals commonly applied in catalysis, nickel is one of the best known (Finiels et al., 2014; Lipshutz et al., 2003; Plumejeau et al., 2015). It is one of the most abundant elements in the Earth's crust and is approximately 5000 times cheaper than gold (De et al., 2016). Due to the long history of the use of nickel in catalysis, the literature on nickel catalysts is vast and covers an enormous number of reactions, including oxidation, reduction, hydrogenation and reforming reactions (Lipshutz, 2001; Lipshutz et al., 2003). Despite the significant success of applications of this element in industry, purely nickel-based catalysts still cannot be used for environmental applications, due to problems with selectivity, stability and activity (Kour et al., 2020; Qin et al., 2020). To overcome these obstacles, nickel–carbon composites have been developed. The use of carbon as a support enables the good dispersion of the metal-containing phase on the support surface. Moreover, the properties of carbonized materials, including high chemical and thermal stability, high porosity, low density and weight, may help to fulfil the strict requirements for environmental applications (De et al., 2016).

The main aim of this study was to prepare novel, 3D fibrous-like nickel-based bio-carbons and test their potential use as catalysts in model reactions. As a source of carbonaceous material, spongin-based scaffolds derived from the marine demosponge *Hippospongia communis* were used. This biopolymer creates unique systems of channels built by interwoven fibres. Spongin chemistry is considered complex. Despite some similarities to collagen and keratin, spongin is distinguished by the presence of halogens (such as I and Br) and xylose. The physicochemical properties of spongin-based scaffolds, including thermal stability, persistence in acidic media and the presence of various heteroatoms, suggest that they can be used as an innovative precursor of bio-carbons, including metallized 3D carbon materials (Petrenko et al., 2019; Szatkowski et al., 2018). In this study, the low-temperature carbonization of spongin-based scaffolds was used to generate hierarchical 3D carbonaceous structures preserving the original morphology of the spongin-based skeleton. The scaffolds underwent modification with nickel compounds via the simple and fast sorption reduction method, to obtain novel catalysts. The resulting nickel–carbon composites were effective catalysts in the reduction and oxidation reactions of various phenolic compounds. The reaction kinetics and the reusability of the prepared catalysts were also investigated, and possible mechanisms of reduction and oxidation were proposed.

2. Materials and methods

2.1. Carbonization

Spongin-based skeletons of the marine sponge *Hippospongia communis* (Porifera: Demospongiae), purchased from INTIB GmbH (Germany), were used as a precursor material. The samples were cleaned in distilled water for 1 h, then moved to an ultrasonic bath for 40 min. The sponge skeletons were then immersed in 3 M HCl in a

Table 1
Comparison of catalytic activity in the reduction of 4-nitrophenol and the oxidation of phenol, using various types of catalysts.

Catalyst	Reaction type	Conditions	Rate constant or oxidation efficiency	Source
NiO Ni_2-Co-O Ni-Co_2-O Co_3O_4	4-nitrophenol reduction	Aqueous solution of 4-NP; T: 25 °C; 0.5 mg/mL of catalyst	0.12 min^{-1} 0.42 min^{-1} 0.60 min^{-1} 0.182 min^{-1}	(Khan et al., 2021)
Nickel nanoparticle/carbon catalysts	4-nitrophenol reduction	Aqueous solution of 4-NP; T: 25 °C; 1 g/L of catalyst	0.172–0.046 min^{-1}	(Martín-Jimeno et al., 2021)
Bimetallic Ag-Au	4-nitrophenol reduction	Aqueous solution of 4-NP; T: 25 °C; 1 g/L of catalyst	0.002 min^{-1}	(Emam et al., 2017)
Ni-Y zeolite	4-nitrophenol reduction	Aqueous solution of 4-NP; T: 25 °C; 1 g/L of catalyst	1.200 min^{-1}	(Mekki et al., 2021)
NiO/carbon nanocomposite	4-nitrophenol reduction	Aqueous solution of 4-NP; T: 27 °C; 0.25–0.5 g/L of catalyst	2.700 min^{-1}	(Somasundaram et al., 2018)
Biomass–metakaolin (PSD/MK_Fe) granular composite	Bisphenol A oxidation	Oxygen pressure: 20 bar, T: 160 °C, initial pH: 5–6; 1.0 g/L of catalyst	>98%	(Juhola et al., 2021)
Cu/activated carbon	pPhenol, o-cresol and 2,5-dimethylphenol oxidation from wastewater	Oxygen pressure 0.61 MPa; T: 148 °C; 3.4 g/L of catalyst, pH = 7.4	88–90%	(Mohite and Garg, 2020)
Zn-CNTs-Cu	4-chlorophenol oxidation	Oxygen pressure 0.5 MPa; T: 150 °C pH 2–7; 0.5 g/L of catalyst	20–99%	(Fu et al., 2021)
Carbon coated ceramic monolith	Oxalic acid oxidation	Oxygen pressure 8 bar; T: 140 °C; 60 mg of catalyst	Up to 55%	(Santos et al., 2021)
Paper-like sintered stainless steel fiber with monolayer graphene fil	Phenol oxidation	Fixed-bed reactor, 4.8 g of catalyst, bed height: 4 cm; temperature 80 °C; V = 2 mL/ min	Up to 100%	(Liu et al., 2020c)

purification process. This process was carried out in three stages; after each stage the solution of HCl was exchanged for a fresh one with a concentration of 3 M. The first and second stages of purification were conducted for 6 h, and the third for 3 h. After the acid purification process, samples were cleaned with distilled water to neutral pH, dried, and cut into smaller pieces. The prepared material was subjected to a carbonization process. Carbonization of spongin-based samples was conducted in an R 50/250/13 tube furnace (Nabertherm, Germany) in a nitrogen atmosphere. The process was carried out in a temperature range from 400 to 600 °C, with a 1 h plateau and a heating rate of 10 °C/min, and cooling by thermal inertia to 50 °C. Before the carbonization process, samples were conditioned for 2 h in a nitrogen atmosphere at a temperature of 20 °C.

2.2. Modification procedure

The method was based on the treatment of carbon materials with a solution of nickel nitrate in a concentration of 5 mg/L. Each sample was placed in a three-neck round-bottom flask filled with 50 mL of nickel nitrate salt solution. The first stage, including sorption, was carried out for 1 h with continuous stirring (800 rpm). Next, the reduction was carried out by dropping into the former solution 50 mL of 0.5 mol/L sodium borohydride at a rate of 5 mL/min. After dosing, the reduction process was continued for an additional 30 min, again with continuous stirring (800 rpm). The sorption and reduction procedures were repeated three times. Finally, the metallized materials were dried at 60 °C.

2.3. Morphological and physicochemical analysis

The crystalline structure of the prepared materials was evaluated by the X-ray diffraction method, using a Rigaku Miniflex 600 analyser (Rigaku, Japan) operating with Cu Kα radiation (α = 1.5418 Å). Patterns were obtained over an angular range of 10–80°. Parameters of the crystalline structure of the samples were calculated using PDXL: Integrated X-Ray Powder Diffraction Software (Rigaku, Japan). The analysis was based on the International Centre for Diffraction Data (ICDD) database.

SEM analysis was performed using an EVO-40 scanning electron microscope (Zeiss, Germany). Transmission electron microscopy (TEM) investigations were carried out using a Hitachi HT7700 microscope (Hitachi, Tokyo, Japan) operating at an accelerating voltage of 120 kV. Materials were prepared in epoxide resin and cut into thin layers using a microtome to prepare specimens. EDS X-ray microanalysis was prepared using a Tescan apparatus (Czech Republic) with Gamma-Tec instrumentation from Princeton Inc. (USA). Energy-dispersive X-ray fluorescence spectrometry (XRF) was carried out using an Epsilon 4 spectrometer equipped with a high-resolution silicon drift detector (SDD), typically 135 eV@ Mn-Kα (Malvern Panalytical, UK).

XPS analysis was performed using a Prevac spectrometer (Prevac Ltd.) with a hemispherical Scienta R4000 electron analyser with a Scienta SAX-100 X-ray source (Al K_α, 1486.6 eV, 0.8 eV band) and an XM 650 X-ray monochromator (0.2 eV band). The pass energy of the analyser was set to 50 eV for the regions (high-resolution spectra) Ni 2p, O 1s and C 1s (with a 50 meV step). The base pressure in the analysis chamber was $5 \cdot 10^{-9}$ mbar, and the pressure during the collection of spectra was not higher than $3 \cdot 10^{-8}$ mbar. The porosity characteristics of the obtained materials were determined by the multipoint BET (Brunauer–Emmett–Teller) method using data for adsorption under relative pressure (p/p_o) obtained with an ASAP 2020 instrument (Micromeritics Instrument Co., USA). FTIR analysis was performed with a Vertex 70 apparatus (Bruker, Germany) using the attenuated total reflection (ATR) method. Electrophoretic mobility was measured using a Zetasizer Nano ZS instrument equipped with an autotitrator (Malvern Instruments Ltd., UK) by analysing 0.01 g of catalyst in 25 mL of 0.001 mol/L sodium chloride solution at 25 °C. Changes in the conductivity and pH values of the suspension were observed during the measurement. The pH of the suspensions was adjusted by an automatic titrator using hydrochloric acid (0.2 mol/L) or sodium hydroxide (0.2 mol/L). The zeta potential was obtained from the electrophoretic mobility by the Smoluchowski equation (Sze et al., 2003).

2.4. Catalytic tests

2.4.1. Reduction of 4-nitrophenol

To evaluate the possible application of the prepared metallized materials, they were used as catalysts in the reduction reaction of 4-nitrophenol (4-NP) to 4-aminophenol (4-AP). This reaction was carried out in a quartz cuvette containing 2.5 mL of 4-nitrophenol solution in water (concentration 10 mmol/L). After adding a water solution of sodium borohydride (0.5 mL with concentration 100 mmol/L) and 5 mg of catalyst, the reaction was started. The reduction progress was measured using a UV–Vis spectrophotometer (Jasco V700, Japan) based on spectra obtained after every 60 s of the reaction. In addition, the kinetics of the reaction were calculated based on the pseudo-first-order kinetic model. The choice of this model is a consequence of the excess quantity of sodium borohydride used during the reaction, which means that its concentration can be assumed constant. The proposed model can be described with Eq. (1):

$$\ln(C_t/C_0) = \ln(C_0) - kt \quad (1)$$

where C_0 and C_t denote the initial concentration of 4-NP and the concentration at time t (min), and k (min^{-1}) denotes the rate constant.

2.4.2. Oxidation of phenol and its derivatives

The oxidation reaction was carried out in a three-neck round-bottom flask placed in a water bath. First, the catalyst (50 mg), phenol (50 mL of water solution at concentration 0.5 mmol) and 1 mL of 31 wt% hydrogen peroxide (H_2O_2) were loaded into the reactor. This mixture was stirred (800 rpm) at 60 °C for 4 h under a reflux condenser and then immediately cooled in an ice bath to stop the reaction. Then methanol was added to the mixture to quench the reaction and remove excess hydrogen peroxide. The HPLC-MS system was used to analyse the efficiency of oxidation. The same starting conditions were used for the oxidation of 4-chlorophenoxyacetic acid and methylchlorophenoxypropionic acid. Due to the exothermic nature of this reaction, the concentration of reagents was kept low. Moreover, the agitation speed, reaction volume and amount of catalyst were chosen to avoid external diffusion problems.

LC analysis was performed using the UltiMate 3000 RSLC chromatographic system from Dionex (Sunnyvale, CA, USA). 5 μL samples were injected into a Hypersil Gold C18 RP analytical column (100 × 2.1 mm × 1.9 μm) (Thermo Scientific, USA). In the typical procedure, the column was kept at 35 °C, and the mobile phase was 5 mM ammonium acetate in water (A) and methanol (B), at a flow rate of 0.2 mL/min. The following gradients were used: 0 min 80% B, 5 min 100% B for phenol, and 0 min 50% B, 5 min 100% B for 4-CPA and MCPP. The LC system was connected to an API 4000 QTRAP triple quadrupole mass spectrometer (AB Sciex, Foster City, CA, USA). Compounds were determined by electrospray ionization mass spectrometry (ESI-MS) in negative ion mode. The analyte was detected using the following settings for the ion source and mass spectrometer: curtain gas 10 psi, nebulizer gas 40 psi, auxiliary gas 40 psi, temperature 200 °C, ion spray voltage −4500 V, collision gas set to medium. For more details, see Supplementary Note 1.

3. Results and discussion

3.1. Physicochemical and morphological analysis

The evaluation of physicochemical properties is an important step in describing a new catalytically active material. The XRD patterns of the

functionalized catalysts and of the carbonized spongin-based supports before functionalization are shown in Fig. 1.

As shown in Fig. 1, the XRD patterns exhibit diffractions characteristic for different phases of nickel, carbon, and silicon dioxide. The XRD patterns of the catalysts (Fig. 1A) do not show significant differences. The nickel phase is represented by the three broad diffraction peaks at 12°, 34° and 60°, which can be indexed respectively to $Ni(OH)_2$ (001), $Ni(OH)_2$ (110) and $Ni(OH)_2$ (003) (JCPDS no. 1011134). The formation of a nickel oxide phase is confirmed by the presence of diffraction peaks derived from the NiO (220) phase at 46° (JCPDS no. 1010095). A small but well visible peak, characteristic for the Ni (111) phase, appeared at 43°, and a peak for Ni (220) at 72° (JCPDS no. 9008509). The diffractogram of the catalyst also contains a broad peak characteristic for C(002) (JCPDS no. 9011577). However, the intensity of this peak is significantly lower than for the corresponding phase in the XRD spectra of the pure supports (Fig. 1B). Also, features derived from various forms of silica (Fig. 1B) are not visible in the XRD pattern of the catalysts. This seems to be a result of the modification process, where the carbonized fibres are covered with a metal-containing phase. The strong effect of nickel atoms and the low content of silica compounds results in a lack of silica features in the XRD diffractogram of the catalysts.

The chemical reduction of nickel ions adsorbed onto the surface of carbonaceous scaffolds is an efficient method of functionalization and is well described in the literature (Chen et al., 2017; Kuang et al., 2001; Sahiner et al., 2010). The SEM + EDS analysis provides information about the surface morphology and chemistry of the examined samples (results are shown in Fig. 2).

From the Ni mapping presented in Fig. 3, it is apparent that the metal-containing phase evenly covers all of the prepared catalysts. The highest efficiency of nickel functionalization was achieved for the $NiO/Ni(OH)_2$/Ni_600 catalyst (26.01% mass of Ni), and the lowest for the sample carbonized at 500 °C (15.19% mass of Ni). The variation in the amount of nickel on the surface of the carbonized materials may be explained by the different ability of the carbonized scaffolds to bind nickel ions during the modification process. As has been described elsewhere (Petrenko et al., 2019; Żółtowska et al., 2021), the increase in carbonization temperature results in the formation of bio-carbons with higher carbon content and decreasing content of other heteroatoms, including sulphur and nitrogen, among others. Consequently, the use as supports of bio-carbons obtained at different carbonization temperatures leads to the formation of composites with different nickel loading. Owing to this fact, and referring to the results obtained in previous studies (Petrenko et al., 2019; Żółtowska et al., 2021), a broad statement can be made that the affinity of nickel ions towards the surface of bio-carbons increases with the content of carbon and the level of graphitization of the carbonized material.

Moreover, XRF analysis was performed to evaluate the elemental composition. The results provide evidence of traces of bromine and iron within the structure of the prepared materials; however, the content of these elements is low. Thus, it is assumed that their presence has no significant effect on the catalytic ability; rather, these elements participate in increasing the diversity of surface functional groups. A detailed discussion is given in Supplementary Note 2, and information regarding the surface functional groups is presented in Supplementary Note 5.

It should be noted that the presence of iron (Fe) and aluminium (Al) is linked to the natural origin of the spongin-based scaffolds (Szatkowski et al., 2017; Jesionowski et al., 2018), while the silicon and calcium, according to previous research (Petrenko et al., 2019), are internal elements of the spongin skeleton. As is shown, the applied purification treatment with HCl acid results in the complete removal of calcium; however, it does not lead to the total removal of silicon species. Thus, carbonized spongin-based scaffolds appear to consist of a naturally occurring composite containing carbon, oxygen, nitrogen, sulphur and silicon traces, aluminium, and iron. For catalytic purposes, the existence of small amounts of silicon dioxide or alumina (less than 1 wt %) does not exclude the use of the bio-carbons as supports. Moreover, the presence of heteroatoms such as sulphur, nitrogen, and iron in the catalyst structure may enhance its catalytic properties (Moosapour Siahkalroudi et al., 2021; Wang et al., 2021).

The results of higher-resolution microscopy analysis (SEM and TEM) of the obtained composites are shown in Fig. 3. SEM images of the spongin-based scaffolds before carbonization and functionalization are compared in Supplementary Note 3.

The results of scanning electron microscopy analysis provide evidence that the functionalization of the carbonaceous supports through reduction of adsorbed nickel particles is an effective method. Consequently, the naturally prefabricated, three-dimensional scaffolds are tightly covered with the metal-containing phase, which forms particular structures. Interestingly, the morphology of the metal-containing phase varies with the support used. For the $NiO/Ni(OH)_2$/Ni_400 material, the metal-containing phase creates needle-like structures with a length of around 3–5 μm (Fig. 3A). For $NiO/Ni(OH)_2$/Ni_500, spherical agglomerates of the metal-containing phase are visible (Fig. 3C), while the surface of $NiO/Ni(OH)_2$/Ni_600 is again characterized by the presence of needle-like structures (Fig. 3E), although these structures are thicker and longer than those observed on the fibres of $NiO/Ni(OH)_2$/Ni_400. These interesting differences in the morphological structure of the catalysts cannot be related to the method of synthesis, because all supports were treated in the same way. A possible explanation of these variations may be differences in the loading of the nickel-containing phase; as was mentioned previously, the material prepared

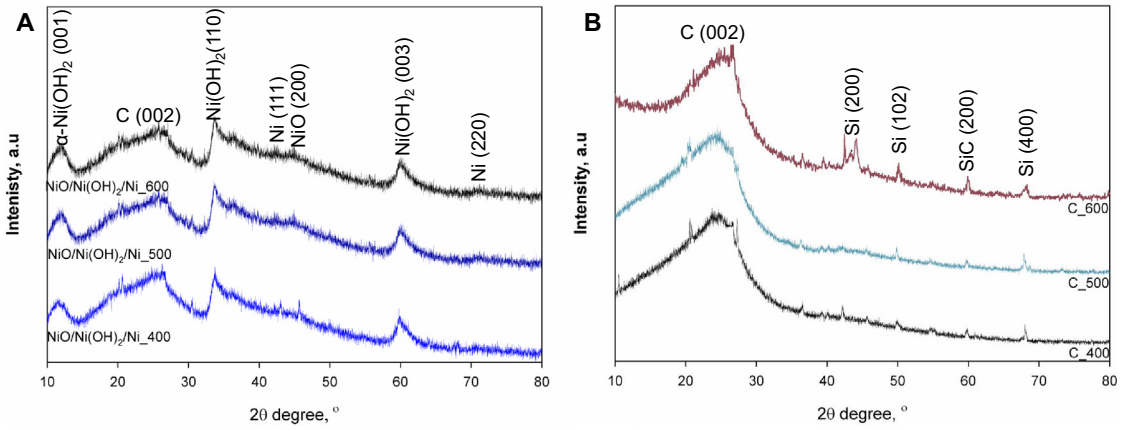

Fig. 1. XRD patterns of the prepared catalysts (A) compared with XRD diffractograms of supports before functionalization (B).

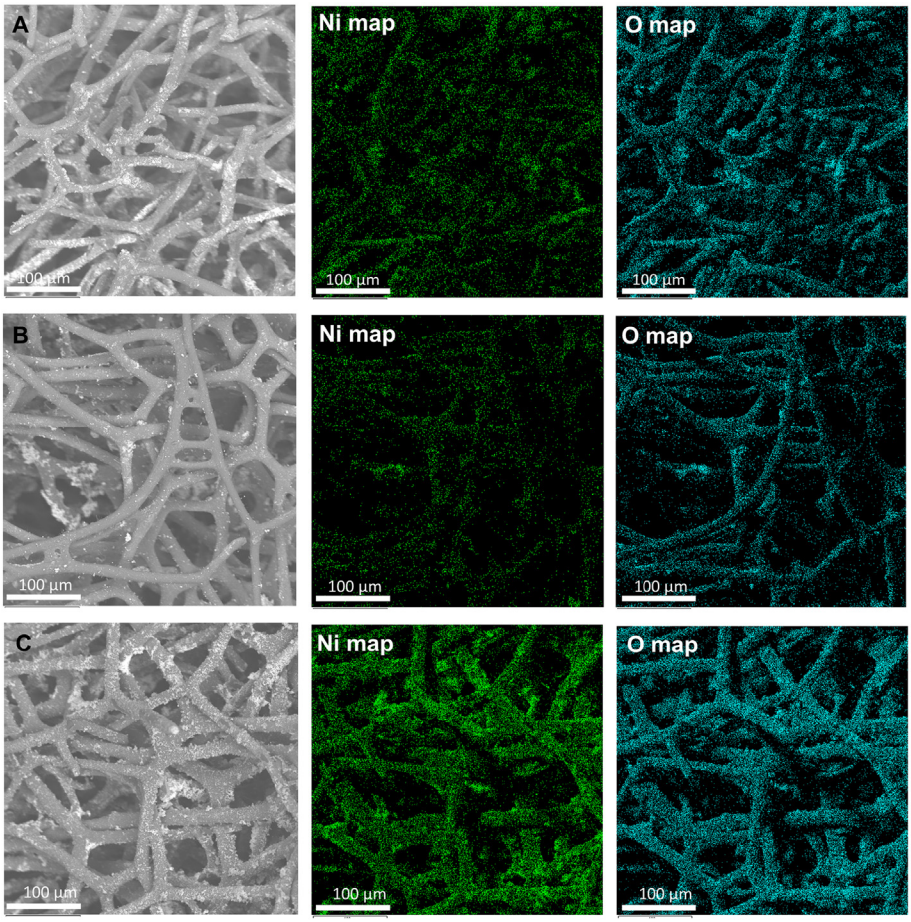

Element	Content [% Wt]
Ni	18.68
C	59.88
N	5.55
S	0.22
O	14.38
Al	0.3
Si	0.71
Fe	0.27

Element	Content [% Wt]
Ni	15.19
C	66.00
N	5.75
S	0.18
O	11.96
Al	0.28
Si	0.63
Fe	-

Element	Content [% Wt]
Ni	26.01
C	55.47
N	8.02
S	0.27
O	9.69
Al	0.33
Si	0.21
Fe	-

Fig. 2. SEM + EDS mapping of NiO/Ni(OH)$_2$/Ni_400 (A), NiO/Ni(OH)$_2$/Ni_500 (B) and NiO/Ni(OH)$_2$/Ni_600 (C) catalysts with the elementary surface composition of the prepared materials.

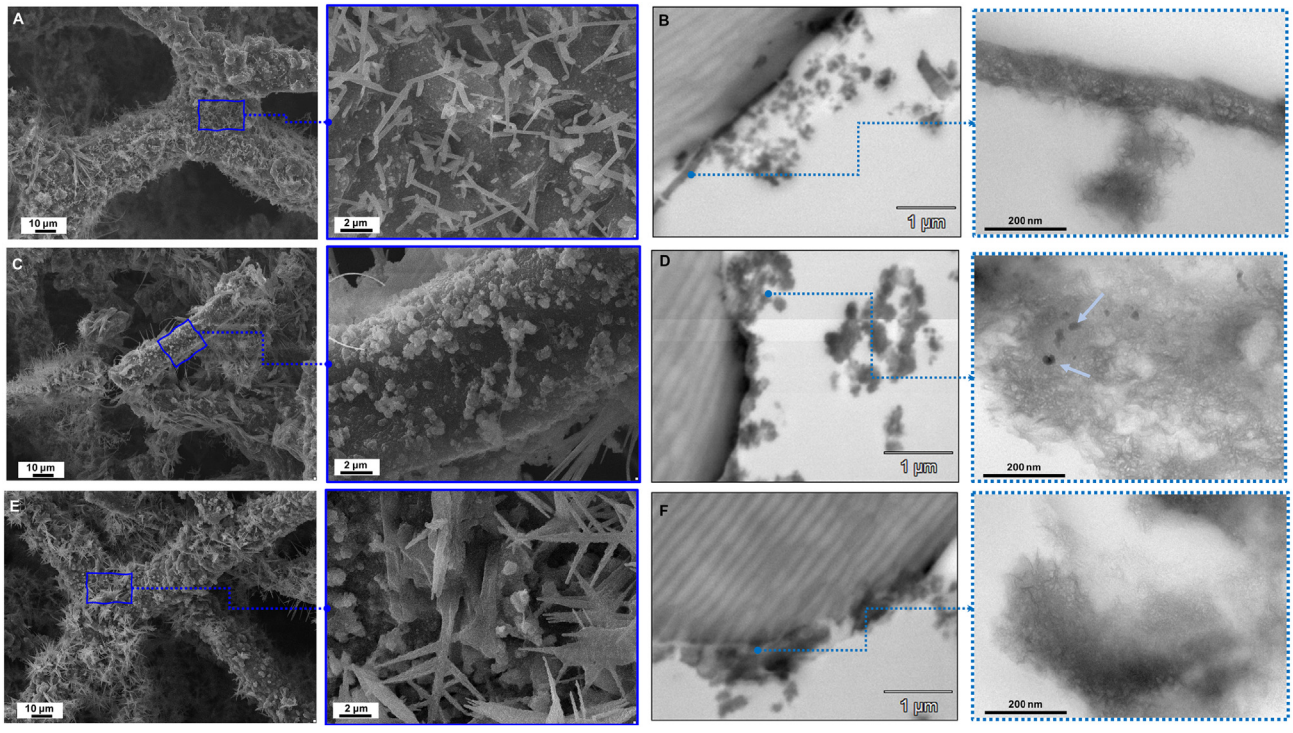

Fig. 3. SEM investigation of prepared materials: NiO/Ni(OH)2/Ni_400 (A), NiO/Ni(OH)2/Ni_500 (C) and NiO/Ni(OH)2/Ni_600 (E) with corresponding TEM images (B, D, F). Images were taken at different magnifications.

using the carbonized support obtained at the highest carbonization temperature seems to have a superior ability to bind the nickel species, and thus the agglomerates formed are larger than in the case of the other materials. Consequently, differences in surface chemistry, such as graphitization level and carbon content, may affect the efficiency of the functionalization process and indirectly the final structure of the metal-containing phase (Petrenko et al., 2019). The influence of surface properties on the loading of the metal-containing phase, as observed in this study, is a well-known phenomenon sufficiently described in other works (Alijani et al., 2021; Peng et al., 2021).

The most promising aspect of the application of carbonized spongin-based scaffolds as a support for the metal-containing phase is their three-dimensional fibrous architecture. The SEM images show a unique structure of interlaced fibres, which usually form channels with diverse shapes: triangle-like, rectangular-like, pentagonal-like and hexagonal-like, with sizes ranging from 1 to 300 μm. These structures are well visible on the SEM images (for comparison, see Fig. 2 and Supplementary Note 3). Therefore, it should be emphasized that the approach proposed in this paper, where the spongin-based scaffold was used as a bio-template together with a simple method of functionalization, led to the obtaining of desirable 3D structures.

The TEM images in Fig. 3B, D, F show the metal-containing phase deposited on the bio-carbon fibres. It can be assumed that in nanoscale, the structure of the metal-containing phase is similar and consists of thin sheets. Moreover, it seems that the modification process results in thick aggregates with irregular structure, forming the metal-containing layer on the surface of the carbonized bio-carbon (Huang et al., 2013). Additionally, in Fig. 3D, some contaminants – derived from silicon dioxide – are marked with arrows.

XPS analysis was carried out to evaluate in detail the surface composition of the prepared catalysts. The spectra obtained are shown in Fig. 4.

The Gaussian fitting method was used for a comprehensive analysis of the oxidation state of the nickel as well as the contributions of oxygen and carbon. In the case of all catalysts, the Ni 2p core-level spectra show two intense peaks at around 855.5 and 871 eV, attributed to Ni $2p_{3/2}$ and Ni $2p_{1/2}$ respectively, with corresponding satellites at around 861.3 and 879.7 eV, characteristic for Ni^{2+} (An et al., 2014; Cheng et al., 2017; Zhou et al., 2017). The core–shell peaks are attributed to Ni—O bonds, in this case associated with the hydroxide, as was confirmed in XRD analysis. The XPS spectra do not show any features corresponding to the NiO phase because its characteristic peaks appear at lower binding energies. These results might be related to additional atmospheric moisture adsorption. The O 1s spectra exhibit three oxygen contributions, labelled O1, O2 and O3. The O1 peak, derived from O–O–C bonds, is located at 534.1 eV (peak area 27.74%) for the NiO/$Ni(OH)_2$/Ni_400 catalyst, 534.0 eV (peak area 10.35%) for NiO/$Ni(OH)_2$/Ni_500 and 534.2 eV (peak area 8.36%) for NiO/$Ni(OH)_2$/Ni_600. Its existence indicates that CO_2 molecules were adsorbed on the surface of each catalyst. The O2 peak is commonly ascribed to physi-/chemisorbed water within the material's interface. The O3 feature, at 531.9 eV (peak area 35.04%) for NiO/$Ni(OH)_2$/Ni_400, 531.3 eV (peak area 44.87%) for NiO/$Ni(OH)_2$/Ni_500 and 534.5 eV (peak area 51.48%) for NiO/$Ni(OH)_2$/Ni_600, is characteristic for metal–oxygen bonds (Payne et al., 2012; Weidler et al., 2017). A comparison of the C 1s spectra is given in Supplementary Note 4.

The presented spectra do not differ significantly in terms of the surface composition, but show differences in the contents of various elements. Such results are not surprising considering the catalyst preparation method. Nevertheless, the XPS results show that NiO/Ni$(OH)_2$/Ni_400 has the highest amount of CO_2 adsorbed on the surface and produces more intense satellite peaks than the NiO/$Ni(OH)_2$/Ni_500 and NiO/$Ni(OH)_2$/Ni_600 catalysts.

Further determination of surface functional groups was performed using FTIR spectroscopy. It was proven that the prepared materials contain various functional groups, including hydroxyl, amino and sulfoxide groups, among others. Besides, the formation of Ni—O groups is indicated (for detailed investigation, see Supplementary Note 5). The effect of pH on the zeta potential was also evaluated to investigate the electrokinetic behaviour of the prepared composites. The results indicate that the contents of nickel species and the electron releasing groups impact the value of the isoelectric point. Consequently, the NiO/$Ni(OH)_2$/Ni_600 material, which has the highest content of nickel moieties, also has the highest IEP. A detailed discussion of the electrokinetic behaviour of the prepared materials is given in Supplementary Note 6.

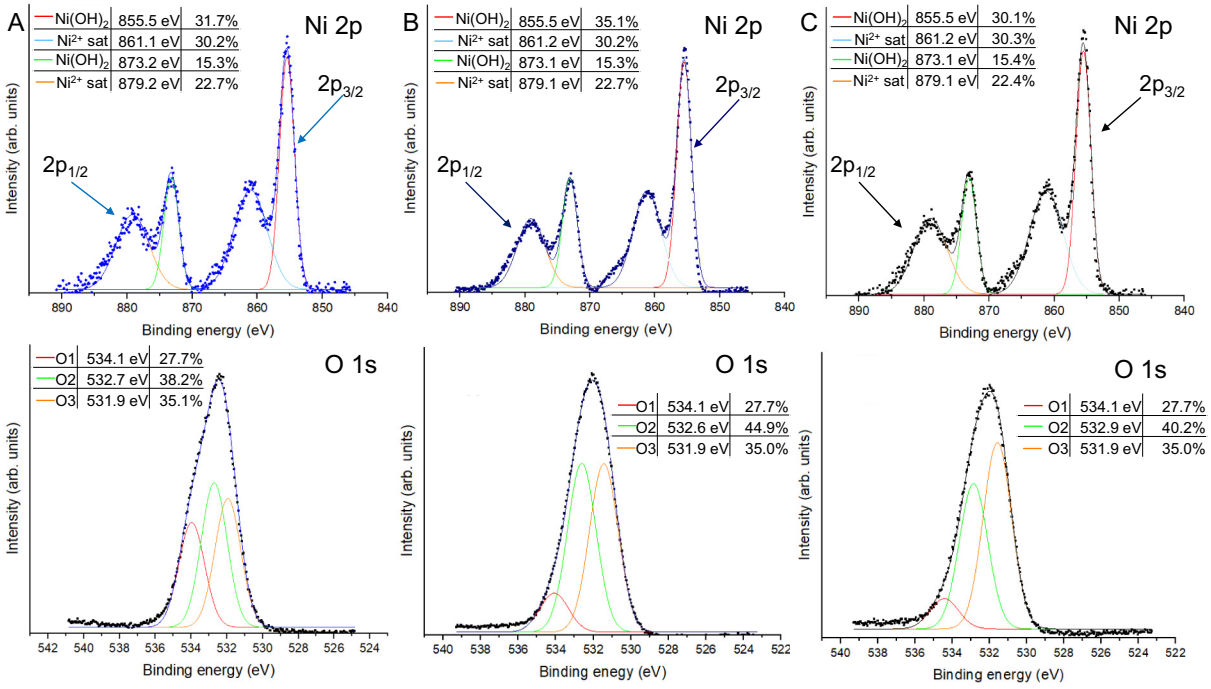

Fig. 4. XPS spectra of Ni 2p and O 1s components of NiO/$Ni(OH)_2$/Ni_400 (A), NiO/$Ni(OH)_2$/Ni_500 (B) and NiO/$Ni(OH)_2$/Ni_600 (C) catalysts.

Fig. 5 presents the porous structure parameters, examined using the low-temperature nitrogen sorption technique.

The nitrogen sorption capacity is highest for the NiO/Ni(OH)$_2$/Ni_500 catalyst. It is slightly lower for NiO/Ni(OH)$_2$/Ni_400 and approximately three times lower for NiO/Ni(OH)$_2$/Ni_600. These results correspond to the decrease in the calculated BET surface area. The sorption isotherms of NiO/Ni(OH)$_2$/Ni_400 and NiO/Ni(OH)$_2$/Ni_500 can be classified as type IV isotherms. The well-visible hysteresis loop suggests that these materials have a mesoporous structure, with pore condensation at high pressure. The NiO/Ni(OH)$_2$/Ni_400 catalyst has the largest pore size among the prepared materials, and NiO/Ni(OH)$_2$/Ni_500 has the highest BET surface area. The isotherms of the NiO/Ni(OH)$_2$/Ni_600 catalyst can be classified as type II, typical for low-porous materials containing both macropores and mesopores but no micropores. This result agrees with the finding that this sample has the lowest surface area.

However, it must be recalled that the method of catalyst preparation results in coverage of the fibres of the carbonized spongin-based scaffolds with the metal-containing phase. For this reason, the surface area of the prepared materials does not exceed 10 m^2/g. As a result, the three-dimensional fibrous support structure with channels of diverse shape may provide good accessibility to the catalyst surface.

3.2. Catalytic evaluation

3.2.1. Reduction of 4-nitrophenol

The catalytic properties of the prepared materials were first tested in the reduction reaction of 4-nitrophenol. This reaction is widely used as a determinant of the catalytic activity of heterogeneous materials, whether or not involving a support (Emam et al., 2017; Grzeschik et al., 2020; Hu et al., 2015; Strachan et al., 2020). Moreover, 4-nitrophenol is an important but toxic substrate used in the production of various drugs, dyes, and pesticides. Therefore, the evaluation of a fast and straightforward method of converting this compound to a functional product is potentially of great benefit from the engineering and environmental point of view (Blaser, 2006).

The UV–Vis spectra (Fig. 6) measured during the reaction in the presence of the prepared catalysts show that all of the tested materials exhibit catalytic ability in the reduction of 4-nitrophenol. The reaction time varies between 4 and 6 min, whereas without the catalyst this reaction does not occur, as explained in Supplementary Note 7. The addition of sodium borohydride led to an increase in the reaction mixture pH from 7 to 10; in such conditions, the functional groups on the surface of the catalysts are deprotonated (see zeta potential measurements in Supplementary Note 4) and are thus negatively charged. Despite the negatively charged surface of the catalyst, only for the NiO/Ni(OH)$_2$/Ni_400 material was an induction period observed; this is apparently related to charging transformation of the surface of the catalyst before reaction (Khalavka et al., 2009; Mahmoud and El-Sayed, 2011; Sarkar et al., 2011; Wu et al., 2011). In the case of the NiO/Ni(OH)$_2$/Ni_500 and NiO/Ni(OH)$_2$/Ni_600 catalysts, different behaviour was observed in the reduction of 4-nitrophenol. For the first-mentioned material, a slow reduction of the peak intensity assigned to the 4-nitrophenolane anion is visible, while for NiO/Ni(OH)$_2$/Ni_600, the peak intensity decreases rapidly after 60 s of the reaction, and the reaction is completed after 4 min. This behaviour may be related to a different path of reduction. For these materials, surface-mediated hydrogen transfer seems to play a leading role during the reduction of 4-nitrophenol.

Because the reducer, sodium borohydride, was applied in significant excess, the kinetics of the reaction were calculated based on the pseudo-first-order kinetic model (Table 2) (Jiang et al., 2012; Sahiner et al., 2010; Yang et al., 2019; Zhu et al., 2011).

The highest reaction rate constant was calculated for the NiO/Ni(OH)$_2$/Ni_400 catalyst. However, the time of reaction is similar for each catalyst used, although the value of the rate constant varies significantly. Even though the highest reaction rate was obtained for the NiO/Ni(OH)$_2$/Ni_400 catalyst, the correlation coefficient took the lowest value. The variations in catalytic activity seem to be related to the structure of the prepared catalyst. The NiO/Ni(OH)$_2$/Ni_400 material has a lower content of nickel phases than NiO/Ni(OH)$_2$/Ni_600, although the needle-like structures observed on the surface of both catalysts are thinner and shorter in the case of NiO/Ni(OH)$_2$/Ni_400 (see Fig. 4A). This may increase the contact area between the reagents and lead to an increase in the diffusion of substrates (Pushkarev et al., 2012; Wang et al., 2014).

Additionally, the NiO/Ni(OH)$_2$/Ni_400 material is characterized by the presence of iron and aluminium, among others, which may create additional active centres of the catalyst. The fact that NiO/Ni(OH)$_2$/Ni_500 has the lowest catalytic activity may therefore be explained by the different morphological structure of the metal-containing phase, together with the lowest content of nickel phases. Since it had the highest rate constant (k), only NiO/Ni(OH)$_2$/Ni_400 was considered for further evaluation of reusability. This material was repeatedly used five times in the catalytic reduction reaction to assess its stability. After each cycle, the catalyst was recovered by filtration, washed several times with deionized water, and dried in a dryer at temperature 60 °C. The calculated rate constants (from the pseudo-first-order model) are compared in Table 2.

Comparison of these data shows a decrease in the rate constant and an increase in the reaction time with each catalytic run, probably because of loss of activity due to the blocking of active sites of the catalyst. On the other hand, it should be noted that after the fifth cycle, the rate constant is still high – comparable to the rate constant obtained for the NiO/Ni(OH)$_2$/Ni_500 catalyst in its first cycle. Such results prove that the formation of a metal-containing phase on the carbonaceous fibrous support provides better stability for the catalytically active phase (Dhokale et al., 2014; Gu et al., 2014; Kongarapu et al., 2017).

The mechanism of 4-nitrophenol reduction is exhaustively described in the literature (Khalavka et al., 2009; Mahmoud and El-Sayed, 2011; Sahiner et al., 2010; Sarkar et al., 2011; Wu et al., 2011). In the description of new catalysts, it is essential to note which

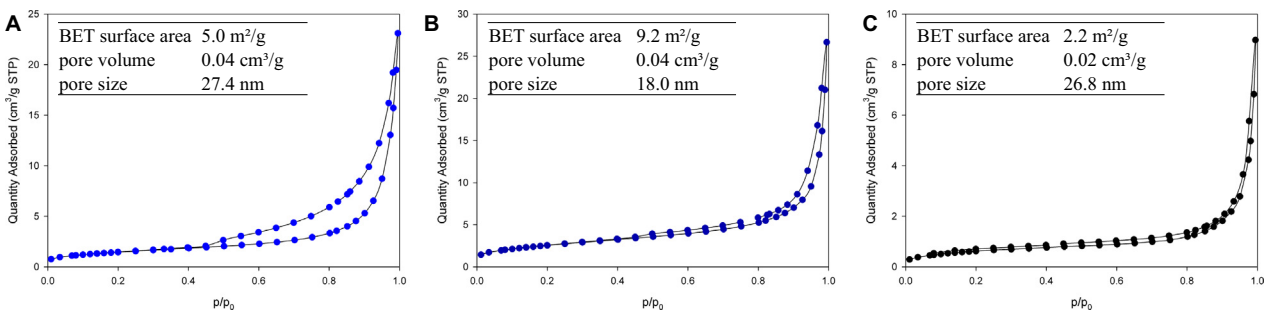

Fig. 5. Nitrogen adsorption isotherms of NiO/Ni(OH)2/Ni_400 (A), NiO/Ni(OH)2/Ni_500 (B) and NiO/Ni(OH)2/Ni_600 (C).

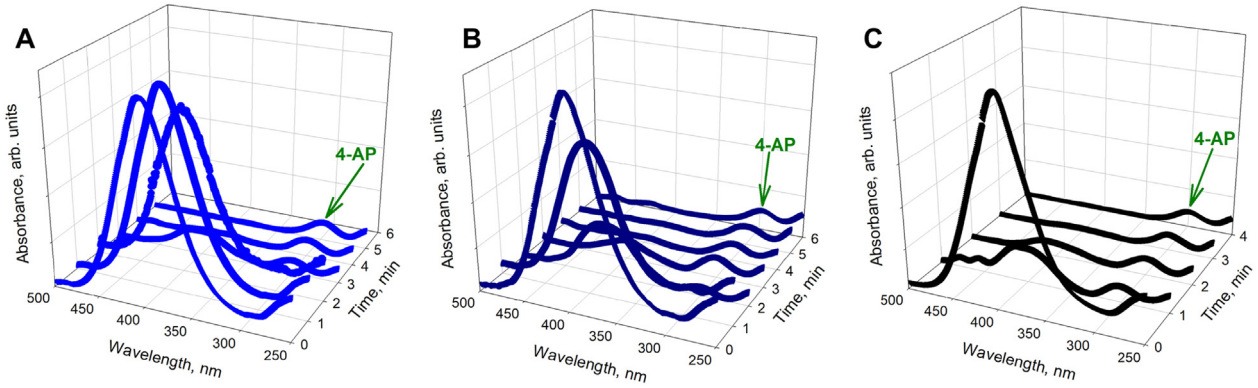

Fig. 6. UV–Vis spectra of reduction of 4-nitrophenol using NiO/Ni(OH)2/Ni_400 (A), NiO/Ni(OH)2/Ni_500 (B), and NiO/Ni(OH)2/Ni_600 (C).

component can be assumed as the active site of the catalyst. Based on the available literature (Wunder et al., 2010, 2011) and the present results, it can be assumed that the reduction occurs by way of sodium borohydride decomposition on the crystallites of nickel moieties. In the next stage, electron transfer occurs from BH_4^- molecules towards 4-nitrophenoloane anions via $Ni(OH)_2$/NiO/Ni grains, which play the role of electron carriers. In view of the previously described activity of carbonized spongin-based scaffolds in the reduction of 4-nitrophenol, this study provides evidence that modification with nickel hydroxide, nickel oxide and nickel leads to enhanced catalytic activity, while the carbonized spongin-based scaffolds and the metal-containing phase act synergistically during the reduction reaction. Besides, the three-dimensional, fibrous-like morphology with open channels enhances the diffusion of substrates towards the surface of the catalyst. The promising results concerning the catalytic activity of the prepared materials further encouraged us to evaluate their effectiveness as catalysts in oxidation reactions.

3.2.2. Oxidation of phenol and its derivatives

Phenol, methylchlorophenoxypropionic acid (MCPP) and 4-chlorophenoxyacetic acid (4-CPA) were used as substrates for the catalytic oxidation reaction. These compounds are commonly used in the production of drugs (phenol) and pesticides (MCPP and 4-CPA). Their presence in water streams has been proved in several studies (Abdel Rahman and Hung, 2020; Somasundaram et al., 2018; Wang et al., 2020; Wang et al., 2016a), as have their toxic and bioaccumulation effects on the environment (Benny and Chakraborty, 2020; Piotrowska et al., 2017). The oxidation was carried out in a water solution at temperature 60 °C in the presence of hydrogen peroxide as an oxidizing agent, for a time of 4 h. The oxidation efficiency was calculated based on measurement of the concentration of the substrate after the reaction, using the calibration curve method. The obtained oxidation efficiencies are shown in Fig. 7.

The above results show the good catalytic ability of NiO/Ni(OH)$_2$/Ni_400. Application of this catalyst at acidic pH leads to full oxidation of MCPP and 4-CPA (oxidation yield more than 99%) and sufficient oxidation of phenol (oxidation yield 80%) (Fig. 7A). Without a catalyst, the yield of oxidation is not higher than 10%. This proves that the presence of a catalyst is essential for the oxidation of phenolic compounds. Interestingly, the NiO/Ni(OH)$_2$/Ni_500 and NiO/Ni(OH)$_2$/Ni_600 catalysts presented significantly weaker catalytic properties. The yield of oxidation of any substrate was not higher than 33%. In contrast to the results for the reduction of 4-nitrophenol, where the difference in catalytic activity was relatively small, the same materials used in oxidation reactions differed significantly in catalytic activity. The favourable catalytic activity of NiO/Ni(OH)$_2$/Ni_400 may be a consequence of the morphology of the metal-containing phase forming the well-dispersed needle-like structure, the fact that it has the largest pore size among the prepared materials, as well as the chemical composition of the bio-carbon. The material obtained at the lowest carbonization temperature exhibits the presence of various heteroatoms, as described in other studies (Petrenko et al., 2019; Żółtowska et al., 2021). Owing to the chemical composition of the prepared composites, the NiO/Ni(OH)$_2$/Ni_400 material has the most diverse elemental composition, with the highest percentage of oxygen, iron, bromine, and iodine. Thus, it can be concluded that this material, thanks to the diversification of its surface functional groups, can create various active centres, enhancing its catalytic activity. However, the nickel-containing phase seems to be the major player in the tailoring of the catalytic properties. Thus, it can be assumed that the morphology of the prepared materials and the nickel content may be the crucial factors impacting the activity of the catalyst. Consequently, as can be seen in Fig. 3, an excessive amount of nickel leads to the formation of larger nickel-containing clusters, but with lower surface area. Related to this assumption, BET data showed a higher surface area for the NiO/Ni(OH)$_2$/Ni_500 material. For this reason, the NiO/Ni(OH)$_2$/Ni_400 surface morphology seems to be the best suited for catalytic purposes.

In the next step, the phenolic compounds were oxidized at alkaline pH (Fig. 7B). The results show that increasing the pH negatively affects the efficiency of oxidation of phenol, MCPP, and 4-CPA. (NiO/Ni(OH)$_2$/Ni_500 was excluded from testing because it had the lowest catalytic activity.) These results may be explained by the fact that in a water solution with pH in the range 2–3, decomposition of hydrogen peroxide produces hydrogen radicals (OH•), which play the leading role in the oxidation of organic compounds (Xing et al., 2018; Zhang et al., 2019). At higher pH, the main product of hydrogen peroxide decomposition is hydroxyl ions. Therefore the concentration of radicals is significantly lower, which results in lower reaction efficiency. The significantly higher catalytic ability of NiO/Ni(OH)$_2$/Ni_400 catalysts may be a result of their having the largest pore size among the materials, and the highest content of surface oxygen and the Ni^{2+} phase together with the presence of other heteroatoms (Fe, Al, S, among others). In consequence, the synergistic action of several factors impacts the final catalytic activity in oxidation reactions.

Table 2
Kinetic parameters of reduction of 4-nitrophenol using the prepared catalysts.

Catalyst	No. of cycle	k (min^{-1})	R^2	Time of reaction (min)
NiO/Ni(OH)$_2$/Ni_400	1	1.022 ± 0.137	0.949	5
	2	0.936 ± 0.135	0.959	5
	3	0.732 ± 0.068	0.975	6
	4	0.635 ± 0.068	0.989	7
	5	0.513 ± 0.020	0.994	9
NiO/Ni(OH)$_2$/Ni_500		0.648 ± 0.065	0.952	6

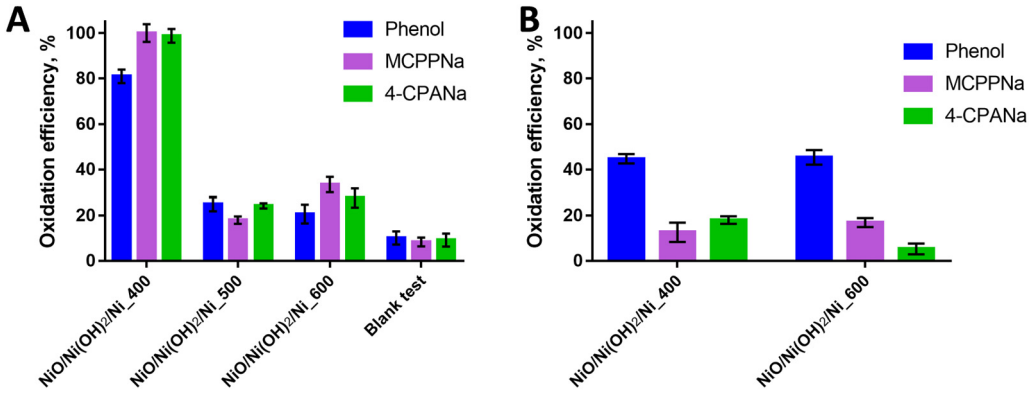

Fig. 7. The efficiency of oxidation of phenol, MCPP, and 4-CPA using various carbonized spongin-based catalysts at pH 3 (A) and pH 8 (B) (concentration of substrate 0.0005 mol/L, catalyst concentration 1 g/L, time of reaction 4 h, 60 °C).

The results of zeta potential measurements can provide further important information on the influence of pH. The pKa value was 9.94 for phenol and 3.56 and 3.75 for 4-CPA and MCPP respectively. It can be concluded that when the pH of the reaction is 3 the compounds are in a protonated state, with the surface groups of each catalyst positively charged. For reactions carried out at pH 8 the 4-CPA and MCPP molecules are deprotonated, while phenol is still in the protonated form, and the catalysts have negatively charged surface functional groups. It appears, therefore, that at acidic pH, the repulsive electrostatic interaction between the catalyst surface and the substrate molecules does not hamper the oxidation process significantly. Moreover, the prepared catalysts are involved in the formation of hydroxyl radicals (at pH 3) or hydroxyl ions (at pH 8), which attract molecules of the phenolic compounds. An increase in the pH of the reaction mixture, therefore, has a significant negative effect on the oxidation efficiency.

As regards possible interactions between the substrates and catalysts, π-π interactions may be considered the most important. However, in the oxidation reactions, the catalyst acts via electron transfer. A more detailed examination of interactions between the substrates and catalysts will not be made here.

To obtain a useful catalyst, not only high catalytic activity is essential. Such a material should also be stable over catalytic cycles. Thus, reusability experiments were carried out to evaluate the possibility of multiple application of the $NiO/Ni(OH)_2/Ni\_400$ material in repeated oxidation of phenol, MCPP, and 4-CPA.

As the results (Fig. 8) show, an apparent decrease in oxidation efficiency is visible in the case of each compound. In the oxidation of MCPP and 4-CPA, the reduction of catalytic ability after the fifth run reaches 80%. The lowest decrease in catalytic activity is observed for the oxidation of phenol, where the catalyst retains 40% of its activity

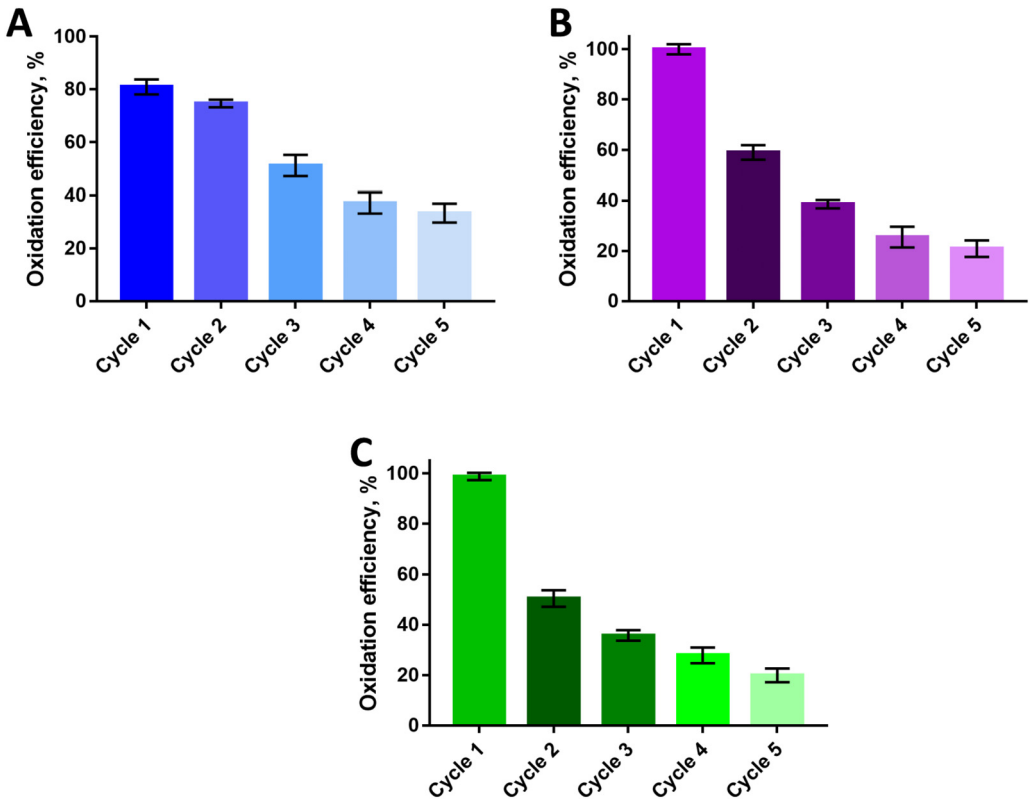

Fig. 8. Changes in oxidation efficiency during catalytic cycles using NiO/Ni(OH)2/Ni_400 catalyst in the oxidation of phenol (A), MCPP (B) and 4-CPA (C) (concentration of substrate 0.0005 mol/L, catalyst concentration 1 g/L, time of reaction 4 h, pH 3, 60 °C).

after the fifth catalytic run. Interestingly, the reaction with this compound gives the lowest yield in the first catalytic cycle. However, after the second, third, fourth, and fifth reaction runs, the calculated activity of NiO/Ni(OH)$_2$/Ni_400 in the oxidation of phenol is higher than for both 4-CPA and MCPP after the same number of runs. The observed reduction in catalytic activity may be related to loss of catalyst mass during the recovery and washing process. However, deactivation of active sites by poisoning could not be excluded. This is the case especially for 4-CPA and MCPP, as the intermediate products of their oxidation contain chlorine, which can act as a poison on the catalyst surface. This assumption may explain the significant decrease in oxidation efficiency on repeated reuse (Mork and Norgard, 1976; Paquin et al., 2015).

Because the mechanism of phenol oxidation is extensively discussed in the literature, it will not be evaluated in detail here. However, to investigate the mechanisms of 4-CPA and MCPP oxidation, MS spectra before and after oxidation were recorded (see Supplementary Note 8).

4. Future perspectives

Evolution in materials science and catalysis has led to work that merges two different topics: metals and biopolymers. There is an increasing number of reports on carbon materials derived from biomass. Most biopolymers (lignin, collagen, silk, cellulose, starch, chitin, chitosan, dextran, pectin, alginate, carrageenan) can be successfully used as precursors of carbon materials (Boury and Plumejeau, 2014; Lee et al., 2011, 2012; Qu et al., 2016; Q. Wang et al., 2016b; Zhao et al., 2016). Biopolymers of biological origin are of particular importance for obtaining carbon materials (Zhang et al., 2010). This is related to their chemical structure, which is rich in heteroatoms such as nitrogen or sulphur; the presence of these increases the diversity of surface functional groups. Therefore, these carbon materials are well suited as scaffolds for metal–carbon composites (Lee et al., 2011, 2012; Zhang et al., 2010).

Among the many biopolymers commonly applied in the preparation of bio-carbons, spongin-based scaffolds seem to be the most promising choice. Spongin belongs to the "collagen suprafamily" (Petrenko et al., 2019), and it is the main skeletal protein building the skeletons of sponges in the class Demospongiae, which can grow up to 70 cm. These spongin-based skeletons have been known since ancient times as natural (bath) or commercial sponges, and have been used for cosmetic or medical purposes. Their use for the preparation of bio-carbons is economically feasible, because they are cultivated under marine farming conditions on a large scale worldwide, creating a sponge market worth more than US$20 million (Żółtowska et al., 2021). Moreover, in contrast to other biomass materials used to prepare bio-carbons, which are fragile and can be applied only in the form of powder, these ready-to-use scaffolds preserve the unique structure of Demospongiae sponge skeletons even after carbonization at temperatures as high as 1200 °C. Carbonized spongin-based scaffolds are mechanically robust and can be used to prepare bio-carbons with a strictly designed shape.

Nevertheless, this study and other recently published work (Petrenko et al., 2019; Żółtowska et al., 2021) are just the beginning of efforts to discover the full potential of bio-carbons derived from spongin-based scaffolds. Further research may focus on the atomistic simulation of bio-carbons to provide an additional overview regarding the optimization of properties. Therefore, significant effort should be put into understanding the mechanism of transformation from organic precursor to inorganic carbon and the effect of additives on the structural and chemical properties of the resulting bio-carbon. Moreover, knowledge of the mechanism of functionalization and effect of the bio-carbon structure on the properties of the resulting composite may provide additional insight and represent a milestone in the development of efficient bioinspired materials. Besides, the detailed characterization of spent catalysts may be considered as a subject of future evaluation, encompassing changes in composite morphology, elemental content, BET surface area, leaching of the metal-containing phase, and deeper catalytic study, including the mechanistic aspects. Likewise, the heat conduction of modified bio-carbon-based composites in catalytic applications is another potential area of research.

Spongin-based scaffolds are indisputably promising materials for use for catalytic purposes. Their carbonization has been shown to lead to bio-carbons with exceptional stability, robustness and physicochemical properties. The relatively simple functionalization method demonstrated in this study, which does not require the use of extreme synthesis conditions or toxic and expensive reagents, opens up new possibilities for the preparation of bio-inspired materials, which is in line with the philosophy of sustainable development.

5. Conclusion

A spongin-based fibrous scaffold isolated from the marine demosponge *Hippospongia communis* was utilized as a precursor of a carbon support and subjected to carbonization (at various temperatures) followed by modification with nickel and nickel oxide. For the first time, a relatively simple method of functionalization of carbonized scaffolds was applied to obtain nickel-based bio-carbon composites. Morphological and physicochemical analysis revealed moderate differences in the chemical nature of the prepared materials. It was shown that the temperature of carbonization influences the effectiveness of the modification process. However, this study mainly focused on the characterization of the prepared materials and their evaluation as potential catalysts for oxidation or reduction reactions of various phenolic compounds. The results confirm the promising activity of all of the materials in the reduction of 4-nitrophenol; the slight differences in the calculated rate constants were ascribed to the different nickel oxide contents in the tested catalysts. The mechanism of reduction was also predicted. In oxidation tests, the NiO/Ni(OH)$_2$/Ni_400 catalyst showed excellent catalytic ability in the oxidation of MCPP and 4-CPA (99% oxidation efficiency at pH 3) and good activity in the oxidation of phenol (80% yield at pH 3). The use of hydrogen peroxide as an oxidizing agent eliminates the formation of additional toxic products of oxidant decomposition.

This remarkable catalytic activity may be ascribed to (i) the diverse chemical composition of the nickel phase, consisting of nickel hydroxide Ni(OH)$_2$, nickel oxide NiO and nickel(0), which creates various active centres of the catalysts; (ii) the even dispersion of the metal-containing phase on the fibres of the carbonized supports; and (iii) the unique needle-like morphology, which acts synergistically with the 3D structure of the supports to provide good diffusion and high contact area between the catalysts and reagents. This study provides evidence that spongin-based scaffolds can be utilized to produce a structured carbonaceous material that can be successfully functionalized with nickel moieties using a simple sorption–reduction approach. As a result, it becomes possible to produce unique composites based on bio-carbon functionalized with nickel species, with impressive catalytic performance in the removal of emerging contaminants.

CRediT authorship contribution statement

Sonia Żółtowska: Conceptualization, Investigation, Writing – original draft, Writing – review & editing, Visualization. **Zuzanna Bielan:** Investigation. **Joanna Zembrzuska:** Investigation, Writing – review & editing. **Katarzyna Siwińska-Ciesielczyk:** Investigation. **Adam Piasecki:** Investigation, Resources. **Anna Zielińska-Jurek:** Investigation. **Teofil Jesionowski:** Supervision, Writing – review & editing, Funding acquisition.

Declaration of competing interest

The authors declare that they have no known competing financial interests or personal relationships that could have appeared to influence the work reported in this paper.

Acknowledgment

The work was supported by the National Science Centre, Poland, project Etiuda no. 2019/32/T/ST8/00414 (S.Ż.), and by the Ministry of Education and Science, Poland (K.S.-C., T.J.). Sonia Żółtowska and Teofil Jesionowski would like to thank Professor Monika Mazik of TU Bergakademie Freiberg for assistance during the catalytic tests.

Appendix A. Supplementary data

Supplementary data to this article can be found online at https://doi.org/10.1016/j.scitotenv.2021.148692.

References

Abdel Maksoud, M.I.A., Elgarahy, A.M., Farrell, C., Al-Muhtaseb, A.H., Rooney, D.W., Osman, A.I., 2020. Insight on water remediation application using magnetic nanomaterials and biosorbents. Coord. Chem. Rev. 403, 213096. https://doi.org/10.1016/j.ccr.2019.213096.

Abdel Rahman, R.O., Hung, Y.T., 2020. Application of ionizing radiation in wastewater treatment: an overview. Water 12, 19. https://doi.org/10.3390/w12010019.

Acharya, R., Parida, K., 2020. A review on TiO_2/g-C_3N_4 visible-light-responsive photocatalysts for sustainable energy generation and environmental remediation. J. Environ. Chem. Eng. 8, 103896. https://doi.org/10.1016/j.jece.2020.103896.

Ahsan, M.A., Jabbari, V., Imam, M.A., Castro, E., Kim, H., Curry, M.L., Valles-Rosales, D.J., Noveron, J.C., 2020. Nanoscale nickel metal organic framework decorated over graphene oxide and carbon nanotubes for water remediation. Sci. Total Environ. 698, 134214. https://doi.org/10.1016/j.scitotenv.2019.134214.

Alijani, S., Capelli, S., Evangelisti, C., Prati, L., Villa, A., Cattaneo, S., 2021. Influence of carbon support properties in the hydrodeoxygenation of vanillin as lignin model compound. Catal. Today 367, 220–227. https://doi.org/10.1016/j.cattod.2020.04.026.

Ambursa, M.M., Juan, J.C., Yahaya, Y., Taufiq-Yap, Y.H., Lin, Y.C., Lee, H.V., 2021. A review on catalytic hydrodeoxygenation of lignin to transportation fuels by using nickel-based catalysts. Renew. Sust. Energ. Rev. 138, 110667. https://doi.org/10.1016/j.rser.2020.110667.

An, C., Wang, Y., Huang, Y., Xu, Y., Jiao, L., Yuan, H., 2014. Porous $NiCo_2O_4$ nanostructures for high performance supercapacitors via a microemulsion technique. Nano Energy 10, 125–134. https://doi.org/10.1016/j.nanoen.2014.09.015.

Bartczak, P., Norman, M., Klapiszewski, Ł., Karwańska, N., Kawalec, M., Baczyńska, M., Wysokowski, M., Zdarta, J., Ciesielczyk, F., Jesionowski, T., 2018. Removal of nickel (II) and lead(II) ions from aqueous solution using peat as a low-cost adsorbent: a kinetic and equilibrium study. Arab. J. Chem. 11, 1209–1222. https://doi.org/10.1016/j.arabjc.2015.07.018.

Benny, C., Chakraborty, S., 2020. Continuous removals of phenol, organics, thiocyanate, and nitrogen in horizontal subsurface flow constructed wetland. J. Water Process Eng. 33, 101099. https://doi.org/10.1016/j.jwpe.2019.101099.

Blaser, H.U., 2006. A golden boost to an old reaction. Science 313, 312–313. https://doi.org/10.1126/science.1131574.

Boury, B., Plumejeau, S., 2014. Metal oxides and polysaccharides: an efficient hybrid association for materials chemistry. Green Chem. 17, 72–88. https://doi.org/10.1039/C4GC00957F.

Chen, H., Liao, F., Yuan, Z., Han, X., Xu, C., 2017. Simple and fast fabrication of conductive silver coatings on carbon fabrics via an electroless plating technique. Mater. Lett. 196, 205–208. https://doi.org/10.1016/j.matlet.2017.03.070.

Chen, Yaoning, Liu, Yuqing, Li, Y., Wu, Y., Chen, Yanrong, Liu, Yihuan, Zhang, J., Xu, F., Li, M., Li, L., 2020. Synthesis, application, and mechanisms of ferro-manganese binary oxide in water remediation: a review. Chem. Eng. J. 388, 124313. https://doi.org/10.1016/j.cej.2020.124313.

Cheng, M., Fan, H., Song, Y., Cui, Y., Wang, R., 2017. Interconnected hierarchical $NiCo_2O_4$ microspheres as high-performance electrode materials for supercapacitors. Dalton Trans. 46, 9201–9209. https://doi.org/10.1039/c7dt01289f.

De, S., Zhang, J., Luque, R., Yan, N., 2016. Ni-based bimetallic heterogeneous catalysts for energy and environmental applications. Energy Environ. Sci. 9, 3314–3347. https://doi.org/10.1039/c6ee02002j.

Dhokale, R.K., Yadav, H.M., Achary, S.N., Delekar, S.D., 2014. Anatase supported nickel nanoparticles for catalytic hydrogenation of 4-nitrophenol. Appl. Surf. Sci. 303, 168–174. https://doi.org/10.1016/j.apsusc.2014.02.135.

El-Sayed, M.E.A., 2020. Nanoadsorbents for water and wastewater remediation. Sci. Total Environ. 739, 139903. https://doi.org/10.1016/j.scitotenv.2020.139903.

Emam, H.E., El-Zawahry, M.M., Ahmed, H.B., 2017. One-pot fabrication of AgNPs, AuNPs and Ag-Au nano-alloy using cellulosic solid support for catalytic reduction application. Carbohydr. Polym 166, 1–13. https://doi.org/10.1016/j.carbpol.2017.02.091.

Fang, Z., Gao, Y., Bolan, N., Shaheen, S.M., Xu, S., Wu, X., Xu, X., Hu, H., Lin, J., Zhang, F., Li, J., Rinklebe, J., Wang, H., 2020. Conversion of biological solid waste to graphene-containing biochar for water remediation: a critical review. Chem. Eng. J. 390, 124611. https://doi.org/10.1016/j.cej.2020.124611.

Finiels, A., Fajula, F., Hulea, V., 2014. Nickel-based solid catalysts for ethylene oligomerization—a review. Catal. Sci. Technol. 4, 2412–2426. https://doi.org/10.1039/c4cy00305e.

Fu, T., Gong, X., Guo, J., Yang, Z., Liu, Y., 2021. Zn-CNTs-Cu catalytic in-situ generation of H_2O_2 for efficient catalytic wet peroxide oxidation of high-concentration 4-chlorophenol. J. Hazard. Mater. 401, 123392. https://doi.org/10.1016/j.jhazmat.2020.123392.

Grzeschik, R., Schäfer, D., Holtum, T., Küpper, S., Hoffmann, A., Schlücker, S., 2020. On the overlooked critical role of the pH value on the kinetics of the 4-nitrophenol $NaBH_4$ - reduction catalyzed by noble-metal nanoparticles (Pt, Pd, and Au). J. Phys. Chem. C 124. https://doi.org/10.1021/acs.jpcc.9b07114.

Gu, X., Qi, W., Xu, X., Sun, Z., Zhang, L., Liu, W., Pan, X., Su, D., 2014. Covalently functionalized carbon nanotube supported Pd nanoparticles for catalytic reduction of 4-nitrophenol. Nanoscale 6, 6609–6616. https://doi.org/10.1039/c4nr00826j.

Hu, Huawen, Xin, J.H., Hu, Hong, Wang, X., Miao, D., Liu, Y., 2015. Synthesis and stabilization of metal nanocatalysts for reduction reactions – a review. J. Mater. Chem. A 3, 11157–11182. https://doi.org/10.1039/c5ta00753d.

Huang, L., Chen, D., Ding, Y., Wang, Z.L., Zeng, Z., Liu, M., 2013. Hybrid composite $Ni(OH)_2$@$NiCo_2O_4$ grown on carbon fiber paper for high-performance supercapacitors. Appl. Mate 5, 11159–11162. https://doi.org/10.1021/am403367u.

Jankowska, K., Ciesielczyk, F., Bachosz, K., Zdarta, J., Kaczorek, E., Jesionowski, T., 2019. Laccase immobilized onto zirconia–silica hybrid doped with Cu^{2+} as an effective biocatalytic system for decolorization of dyes. Materials 12 (8), 1252. https://doi.org/10.3390/ma12081252.

Jesionowski, T., Norman, M., Żółtowska-Aksamitowska, S., Petrenko, I., Joseph, Y., Ehrlich, H., 2018. Marine spongin: naturally prefabricated 3D scaffold-based biomaterial. Mar. Drugs 16, 1–23. https://doi.org/10.3390/md16030088.

Jiang, Z., Xie, J., Jiang, D., Jing, J., Qin, H., 2012. Facile route fabrication of nano-Ni core mesoporous-silica shell particles with high catalytic activity towards 4-nitrophenol reduction. CrystEngComm 14, 4601–4611. https://doi.org/10.1039/c2ce25205h.

Juhola, R., Heponiemi, A., Tuomikoski, S., Hu, T., Huuhtanen, M., Bergna, D., Lassi, U., 2021. Preparation of granulated biomass carbon catalysts – structure tailoring, characterization, and use in catalytic wet air oxidation of bisphenol A. Catalysts 11, 1–20. https://doi.org/10.3390/catal11020251.

Khalavka, Y., Becker, J., Sönnichsen, C., 2009. Synthesis of rod-shaped gold nanorattles with improved plasmon sensitivity and catalytic activity. J. Am. Chem. Soc. 131, 1871–1875. https://doi.org/10.1021/ja806766w.

Khan, A., Wei, D., Wang, Z., Su, X., Wang, J., Alam, S., Wang, L., Wu, R., Maloletnev, A.S., Yang, C., 2021. MOF-derived nickel—cobalt bimetal oxide nanostructures as a cooperative catalyst for the reduction of 4-nitrophenol. J. Chem. Technol. Biotechnol. 96, 697–703. https://doi.org/10.1002/jctb.6582.

Kongarapu, R.J., Mahamallik, P., Pal, A., 2017. Surfactant modification of chitosan hydrogel beads for Ni@NiO core-shell nanoparticles formation and its catalysis to 4-nitrophenol reduction. J. Environ. Chem. Eng. 5, 1321–1329. https://doi.org/10.1016/j.jece.2017.02.017.

Kour, S., Mishra, A., Sinha, A., Kaur, P., Singh, H., 2020. The development of mesoporous Ni-based catalysts and evaluation of their catalytic and photocatalytic applications. ChemistrySelect 5, 3710–3723. https://doi.org/10.1002/slct.201904550.

Kuang, Y., He, N., Wang, J., Xiao, P., Yuan, C., Lu, Z., 2001. Investigating the state of Fe and La in MCM-41 mesoporous molecular sieve materials. Colloids Surf. A Physicochem. Eng. Asp. 179, 177–184. https://doi.org/10.1016/S0927-7757(00)00654-3.

Kubiak, A., Bielan, Z., Kubacka, M., Gabała, E., Zgoła-Grześkowaniak, A., Janczarek, M., Zalas, M., Zielińska-Jurek, A., Siwińska-Ciesielczyk, K., Jesionowski, T., 2020. Microwave-assisted synthesis of a TiO_2-CuO heterojunction with enhanced photocatalytic activity against tetracycline. Appl. Surf. Sci. 520, 146344. https://doi.org/10.1016/j.apsusc.2020.146344.

Kumari, P., Bahadur, N., Dumée, L.F., 2020. Photo-catalytic membrane reactors for the remediation of persistent organic pollutants – a review. Sep. Purif. Technol. 230, 115878. https://doi.org/10.1016/j.seppur.2019.115878.

Lee, H., Lee, D., 2020. Synthesis chemistry and properties of Ni catalysts fabricated on SiC@Al_2O_3 core-shell microstructure for methane steam reforming. Catalysts 10, 391. https://doi.org/10.3390/catal10040391.

Lee, Y.H., Lee, Y.F., Chang, K.H., Hu, C.C., 2011. Synthesis of N-doped carbon nanosheets from collagen for electrochemical energy storage/conversion systems. Electrochem. Commun. 13, 50–53. https://doi.org/10.1016/j.elecom.2010.11.010.

Lee, Y.H., Li, F., Chang, K.H., Hu, C.C., Ohsaka, T., 2012. Novel synthesis of N-doped porous carbons from collagen for electrocatalytic production of H_2O_2. Appl. Catal. B Environ. 126, 208–214. https://doi.org/10.1016/j.apcatb.2012.06.031.

Lipshutz, B.H., 2001. Development of nickel-on-charcoal as a "Dirt-Cheap" heterogeneous catalyst: a personal account. Adv. Synth. Catal. 343, 313–326. https://doi.org/10.1002/1615-4169(20010430)343:4<313::AID-ADSC313>3.0.CO;2-A.

Lipshutz, B.H., Tasler, S., Chrisman, W., Spliethoff, B., Tesche, B., 2003. On the nature of the heterogeneous catalyst: nickel-on-charcoal. J. Organomet. Chem. 68, 1177–1189. https://doi.org/10.1021/jo020296m.

Liu, H., Liu, Y., Tang, L., Wang, J., Yu, J., Zhang, H., Yu, M., Zou, J., Xie, Q., 2020a. Egg shell biochar-based green catalysts for the removal of organic pollutants by activating persulfate. Sci. Total Environ. 745, 141095. https://doi.org/10.1016/j.scitotenv.2020.141095.

Liu, X., Yang, L., Zhao, H., Wang, W., 2020b. Pyrolytic production of zerovalent iron nanoparticles supported on rice husk-derived biochar: simple, in situ synthesis and use for remediation of Cr(VI)-polluted soils. Sci. Total Environ. 708, 134479. https://doi.org/10.1016/j.scitotenv.2019.134479.

Liu, F., Zhang, H., Yan, Y., Huang, H., 2020c. Graphene as efficient and robust catalysts for catalytic wet peroxide oxidation of phenol in a continuous fixed-bed reactor. Sci. Total Environ. 701, 134772. https://doi.org/10.1016/j.scitotenv.2019.134772.

Lu, F., Astruc, D., 2020. Nanocatalysts and other nanomaterials for water remediation from organic pollutants. Coord. Chem. Rev. 408, 213180. https://doi.org/10.1016/j.ccr.2020.213180.

Ma, Y., Hu, K., Sun, Y., Iqbal, K., Bai, Z., Wang, C., Jia, X., Ye, W., 2019. N-doped carbon coated Mn_3O_4/PdCu nanocomposite as a high-performance catalyst for 4-

nitrophenol reduction. Sci. Total Environ. 696, 134013. https://doi.org/10.1016/j.scitotenv.2019.134013.
Mahmoud, M.A., El-Sayed, M.A., 2011. Time dependence and signs of the shift of the surface plasmon resonance frequency in nanocages elucidate the nanocatalysis mechanism in hollow nanoparticles. Nano Lett. 11, 946–953. https://doi.org/10.1021/nl103265s.
Martín-Jimeno, F.J., Suárez-García, F., Paredes, J.I., Martínez-Alonso, A., Tascón, J.M.D., 2021. Nickel nanoparticle/carbon catalysts derived from a novel aqueous-synthesized metal-organic framework for nitroarene reduction. J. Alloys Compd. 853. https://doi.org/10.1016/j.jallcom.2020.157348.
Mekki, A., Mokhtar, A., Hachemaoui, M., Beldjilali, M., Meliani, M. fethia, Zahmani, H.H., Hacini, S., Boukoussa, B., 2021. Fe and Ni nanoparticles-loaded zeolites as effective catalysts for catalytic reduction of organic pollutants. Microporous Mesoporous Mater. 310, 110597. https://doi.org/10.1016/j.micromeso.2020.110597.
Mohite, R., Garg, A., 2020. Performance of supported copper catalysts for oxidative degradation of phenolics in aqueous medium: optimization of reaction conditions, kinetics, catalyst stability, characterization, and reusability. Ind. Eng. Chem. Res. 59, 12986–12998. https://doi.org/10.1021/acs.iecr.0c02211.
Moosapour Siahkalroudi, Z., Aghabarari, B., Vaezi, M., Rodríguez-Castellón, E., Martínez-Huerta, M.V., 2021. Effect of secondary heteroatom (S, P) in N-doped reduced graphene oxide catalysts to oxygen reduction reaction. Mol. Catal 502, 1–9. https://doi.org/10.1016/j.mcat.2020.111372.
Mork, P.C., Norgard, D., 1976. Nickel-catalyzed hydrogenation: a study of the poisoning effect of halogen-containing compounds. J. Am. Oil Chem. Soc. 53, 506–510. https://doi.org/10.1007/BF02636824.
Paquin, F., Rivnay, J., Salleo, A., Stingelin, N., Silva, C., 2015. Multi-phase semicrystalline microstructures drive exciton dissociation in neat plastic semiconductors. J. Mater. Chem. C 3, 10715–10722. https://doi.org/10.1039/b000000x.
Parmeggiani, C., Cardona, F., 2012. Transition metal based catalysts in the aerobic oxidation of alcohols. Green Chem. 14, 547–564. https://doi.org/10.1039/c2gc16344f.
Payne, B.P., Biesinger, M.C., McIntyre, N.S., 2012. Use of oxygen/nickel ratios in the XPS characterisation of oxide phases on nickel metal and nickel alloy surfaces. J. Electron Spectros. Relat. Phenomena 185, 159–166. https://doi.org/10.1016/j.elspec.2012.06.008.
Peng, Y., Sun, Y., Hanif, A., Shang, J., Shen, Z., Hou, D., Zhou, Y., Chen, Q., Ok, Y.S., Tsang, D.C.W., 2021. Design and fabrication of exfoliated Mg/Al layered double hydroxides on biochar support. J. Clean. Prod. 289, 125142. https://doi.org/10.1016/j.jclepro.2020.125142.
Petrenko, I., Summers, A.P., Simon, P., Żółtowska-Aksamitowska, S., Motylenko, M., Schimpf, C., Rafaja, D., Roth, F., Kummer, K., Brendler, E., Pokrovsky, O.S., Galli, R., Wysokowski, M., Meissner, H., Niederschlag, E., Joseph, Y., Molodtsov, S., Ereskovsky, A., Sivkov, V., Nekipelov, S., Petrova, O., Volkova, O., Bertau, M., Kraft, M., Rogalev, A., Kopani, M., Jesionowski, T., Ehrlich, H., 2019. Extreme biomimetics: preservation of molecular detail in centimeter-scale samples of biological meshes laid down by sponges. Sci. Adv. 5, 1–12. https://doi.org/10.1126/sciadv.aax2805.
Piotrowska, A., Syguda, A., Wyrwas, B., Chrzanowski, Ł., Heipieper, H.J., 2017. Toxicity evaluation of selected ammonium-based ionic liquid forms with MCPP and dicamba moieties on *Pseudomonas putida*. Chemosphere 167, 114–119. https://doi.org/10.1016/j.chemosphere.2016.09.140.
Plumejeau, S., Alauzun, J.G., Boury, B., 2015. Hybrid metal oxide@biopolymer materials precursors of metal oxides and metal oxide-carbon composites. J. Ceram. Soc. Japan 123, 695–708. https://doi.org/10.2109/jcersj2.123.695.
Pushkarev, V.V., An, K., Alayoglu, S., Beaumont, S.K., Somorjai, G.A., 2012. Hydrogenation of benzene and toluene over size controlled Pt/SBA-15 catalysts: elucidation of the Pt particle size effect on reaction kinetics. J. Catal. 292, 64–72. https://doi.org/10.1016/j.jcat.2012.04.022.
Qin, Z., Chen, J., Xie, X., Luo, X., Su, T., Ji, H., 2020. CO_2 reforming of CH_4 to syngas over nickel-based catalysts. Environ. Chem. Lett. 18, 997–1017. https://doi.org/10.1007/s10311-020-00996-w.
Qu, W., Xue, Y., Gao, Y., Rover, M., Bai, X., 2016. Repolymerization of pyrolytic lignin for producing carbon fiber with improved properties. Biomass Bioenergy 95, 19–26. https://doi.org/10.1016/j.biombioe.2016.09.013.
Sahiner, N., Ozay, H., Ozay, O., Aktas, N., 2010. New catalytic route: hydrogels as templates and reactors for in situ Ni nanoparticle synthesis and usage in the reduction of 2- and 4-nitrophenols. Appl. Catal. A Gen. 385, 201–207. https://doi.org/10.1016/j.apcata.2010.07.004.
Santos, D.F.M., Soares, O.S.G.P., Silva, A.M.T., Figueiredo, J.L., Pereira, M.F.R., 2021. Degradation and mineralization of oxalic acid using catalytic wet oxidation over carbon coated ceramic monoliths. J. Environ. Chem. Eng. 9, 105369. https://doi.org/10.1016/j.jece.2021.105369.
Sarkar, S., Sinha, A.K., Pradhan, M., Basu, M., Negishi, Y., Pal, T., 2011. Redox transmetalation of prickly nickel nanowires for morphology controlled hierarchical synthesis of nickel/gold nanostructures for enhanced catalytic activity and SERS responsive functional material. J. Phys. Chem. C 115, 1659–1673. https://doi.org/10.1021/jp109572c.
Schmitt, A., Mendret, J., Roustan, M., Brosillon, S., 2020. Ozonation using hollow fiber contactor technology and its perspectives for micropollutants removal in water: a review. Sci. Total Environ. 729, 138664. https://doi.org/10.1016/j.scitotenv.2020.138664.
Siwińska-Ciesielczyk, K., Świgoń, D., Rychtowski, P., Moszyński, D., Zgoła-Grześkowiak, A., Jesionowski, T., 2020. The performance of multicomponent oxide systems based on TiO_2, ZrO_2 and SiO_2 in the photocatalytic degradation of rhodamine B: mechanism and kinetic studies. Colloids Surf. A-Physicochem. Eng. Asp. 586, 124272. https://doi.org/10.1016/j.colsurfa.2019.124272.
Somasundaram, S., Ill-Min, C., Vanaraj, R., Ramaganthan, B., Mayakrishnan, G., 2018. Highly active and reducing agent-free preparation of cost-effective NiO-based carbon nanocomposite and its application in reduction reactions under mild conditions. J. Ind. Eng. Chem. 60, 91–101. https://doi.org/10.1016/j.jiec.2017.10.006.
Strachan, J., Barnett, C., Masters, A.F., Maschmeyer, T., 2020. 4-Nitrophenol reduction: probing the putative mechanism of the model reaction. ACS Catal. 10, 5516–5521. https://doi.org/10.1021/acscatal.0c00725.
Szatkowski, T., Siwińska-Stefańska, K., Wysokowski, M., Stelling, A.L., Joseph, Y., Ehrlich, H., Jesionowski, T., 2017. Immobilization of titanium(IV) oxide onto 3D spongin scaffolds of marine sponge origin according to extreme biomimetics principles for removal of C.I. basic blue 9. Biomimetics 2 (4). https://doi.org/10.3390/biomimetics2020004.
Szatkowski, T., Kopczyński, K., Motylenko, M., Borrmann, H., Mania, B., Graś, M., Lota, G., Bazhenov, V.V., Rafaja, D., Roth, F., Weise, J., Langer, E., Wysokowski, M., Żółtowska-Aksamitowska, S., Petrenko, I., Molodtsov, S.L., Hubálková, J., Aneziris, C.G., Joseph, Y., Stelling, A.L., Ehrlich, H., Jesionowski, T., 2018. Extreme biomimetics: a carbonized 3D spongin scaffold as a novel support for nanostructured manganese oxide(IV) and its electrochemical applications. Nano Res. 11, 4199–4214. https://doi.org/10.1007/s12274-018-2008-x.
Sze, A., Erickson, D., Ren, L., Li, D., 2003. Zeta-potential measurement using the Smoluchowski equation and the slope of the current-time relationship in electroosmotic flow. J. Colloid Interface Sci. 261, 402–410. https://doi.org/10.1016/S0021-9797(03)00142-5.
Verdine, J.C., 2019. Metal oxides in heterogeneous oxidation catalysis: state of the art and challenges for a more sustainable world. ChemSusChem 12 (3), 577–588. https://doi.org/10.1002/cssc.201802248.
Wang, Z., Xu, C., Gao, G., Li, X., 2014. Facile synthesis of well-dispersed Pd-graphene nanohybrids and their catalytic properties in 4-nitrophenol reduction. RSC Adv. 4, 13644–13651. https://doi.org/10.1039/c3ra47721e.
Wang, N., Zheng, T., Zhang, G., Wang, P., 2016a. A review on Fenton-like processes for organic wastewater treatment. J. Environ. Chem. Eng. 4, 762–787. https://doi.org/10.1016/j.jece.2015.12.016.
Wang, Q., Yanzhang, R., Wu, Y., Zhu, H., Zhang, J., Du, M., Zhang, M., Wang, L., Zhang, X., Liang, X., 2016b. Silk-derived graphene-like carbon with high electrocatalytic activity for oxygen reduction reaction. RSC Adv. 6, 34219–34224. https://doi.org/10.1039/c6ra07075b.
Wang, J., de Ridder, D., van der Wal, A., Sutton, N.B., 2020. Harnessing biodegradation potential of rapid sand filtration for organic micropollutant removal from drinking water: a review. Crit. Rev. Environ. Sci. Technol., 1–33 https://doi.org/10.1080/10643389.2020.1771888.
Wang, X., Meng, L., Li, B., Gong, Y., 2021. Heteroatoms/molecules to tune the properties of 2D materials. Mater. Today, 1–23 https://doi.org/10.1016/j.mattod.2020.12.019 article in press.
Weidler, N., Schuch, J., Knaus, F., Stenner, P., Hoch, S., Maljusch, A., Schäfer, R., Kaiser, B., Jaegermann, W., 2017. X-ray photoelectron spectroscopic investigation of plasma-enhanced chemical vapor deposited NiO_x, $NiO_x(OH)_y$, and $CoNiO_x(OH)_y$: influence of the chemical composition on the catalytic activity for the oxygen evolution reaction. J. Phys. Chem. C 121, 6455–6463. https://doi.org/10.1021/acs.jpcc.6b12652.
Wu, K.L., Wei, X.W., Zhou, X.M., Wu, D.H., Liu, X.W., Ye, Y., Wang, Q., 2011. $NiCo_2$ alloys: controllable synthesis, magnetic properties, and catalytic applications in reduction of 4-nitrophenol. J. Phys. Chem. C 115, 16268–16274. https://doi.org/10.1021/jp201660w.
Wunder, S., Polzer, F., Lu, Y., Mei, Y., Ballauff, M., 2010. Kinetic analysis of catalytic reduction of 4-nitrophenol by metallic nanoparticles immobilized in spherical polyelectrolyte brushes. J. Phys. Chem. C 114, 8814–8820. https://doi.org/10.1021/jp101125j.
Wunder, S., Lu, Y., Albrecht, M., Ballauff, M., 2011. Catalytic activity of faceted gold nanoparticles studied by a model reaction: evidence for substrate-induced surface restructuring. ACS Catal. 1, 908–916. https://doi.org/10.1021/cs200208a.
Xing, M., Xu, W., Dong, C., Bai, Y., Zeng, J., Zhou, Y., Zhang, J., Yin, Y., 2018. Metal sulfides as excellent co-catalysts for H_2O_2 decomposition in advanced oxidation processes. Chem 4, 1359–1372. https://doi.org/10.1016/j.chempr.2018.03.002.
Yan, Y., Xia, B.Y., Zhao, B., Wang, X., 2016. A review on noble-metal-free bifunctional heterogeneous catalysts for overall electrochemical water splitting. J. Mater. Chem. A 4, 17587–17603. https://doi.org/10.1039/C6TA08075H.
Yang, F., Shao, B., Liu, X., Gao, S., Hu, X., Xu, M., Wang, Y., Zhou, S., Kong, Y., 2019. Nanosheet-like Ni-based metasilicate towards the regulated catalytic activity in styrene oxidation via introducing heteroatom metal. Appl. Surf. Sci. 471, 822–834. https://doi.org/10.1016/j.apsusc.2018.12.074.
Zdarta, J., Meyer, A.S., Jesionowski, T., Pinelo, M., 2019. Multi-faceted strategy based on enzyme immobilization with reactant adsorption and membrane technology for biocatalytic removal of pollutants: a critical review. Biotechnol. Adv. 37 (7), 107401. https://doi.org/10.1016/j.biotechadv.2019.05.007.
Zhang, L., Jiang, S.P., Wang, W., Zhang, Y., 2007. NiO/YSZ, anode-supported, thin-electrolyte, solid oxide fuel cells fabricated by gel casting. J. Power Sources 170, 55–60. https://doi.org/10.1016/j.jpowsour.2007.03.080.
Zhang, L.-S., Liang, X.-Q., Song, W.-G., Wu, Z.-Y., 2010. Identification of the nitrogen species on N-doped graphene layers and Pt/NG composite catalyst for direct methanol fuel cell. Phys. Chem. Chem. Phys. 12, 12055–12059. https://doi.org/10.1039/c0cp00789g.
Zhang, Y., Zhang, N., Wang, T., Huang, H., Chen, Y., Li, Z., Zou, Z., 2019. Heterogeneous degradation of organic contaminants in the photo-Fenton reaction employing pure cubic B-Fe_2O_3. Appl. Catal. B Environ. 245, 410–419. https://doi.org/10.1016/j.apcatb.2019.01.003.
Zhao, Z., Cannon, F.S., Nieto-Delgado, C., Pena, L., 2016. Lignin/collagen hybrid biomaterials as binder substitute for specialty graphites and electrodes. Carbon 108, 303–317. https://doi.org/10.1016/j.carbon.2016.07.026.

Zheng, Y., Zhu, B., Chen, H., You, W., Jiang, C., Yu, J., 2017. Hierarchical flower-like nickel (II) oxide microspheres with high adsorption capacity of Congo red in water. J. Colloid Interface Sci. 504, 688–696. https://doi.org/10.1016/j.jcis.2017.06.014.

Zhou, T., Cao, Z., Zhang, P., Ma, H., Gao, Z., Wang, H., Lu, Y., He, J., Zhao, Y., 2017. Transition metal ions regulated oxygen evolution reaction performance of Ni-based hydroxides hierarchical nanoarrays. Sci. Rep. 7, 1–9. https://doi.org/10.1038/srep46154.

Zhu, Z., Guo, X., Wu, S., Zhang, R., Wang, J., Li, L., 2011. Preparation of nickel nanoparticles in spherical polyelectrolyte brush nanoreactor and their catalytic activity. Ind. Eng. Chem. Res. 50, 13848–13853. https://doi.org/10.1021/ie2017306.

Żółtowska, S., Koltsov, I., Alejski, K., Ehrlich, H., Ciałkowski, M., Jesionowski, T., 2021. Thermal decomposition behaviour and numerical fitting for the pyrolysis kinetics of 3D spongin-based scaffolds. The classic approach. Polym. Test. 97, 107148. https://doi.org/10.1016/j.polymertesting.2021.107148.

Żółtowska-Aksamitowska, S., Bartczak, P., Zembrzuska, J., Jesionowski, T., 2018. Removal of hazardous non-steroidal anti-inflammatory drugs from aqueous solutions by biosorbent based on chitin and lignin. Sci. Total Environ. 612, 1223–1233. https://doi.org/10.1016/j.scitotenv.2017.09.037.

Zuo, W., Yu, G., Dong, Z., 2016. A MOF-derived nickel based N-doped mesoporous carbon catalyst with high catalytic activity for the reduction of nitroarenes. RSC Adv. 6, 11749–11753. https://doi.org/10.1039/c5ra23082a.